Available online at www.sciencedirect.com
SCIENCE DIRECT®
International Journal of Solids and Structures 41 (2004) 7361–7375
INTERNATIONAL JOURNAL OF SOLIDS and STRUCTURES
www.elsevier.com/locate/ijsolstr

Wave transmission characteristics in periodic media of finite length: multilayers and fiber arrays

F. Kobayashi, S. Biwa *, N. Ohno

Department of Micro System Engineering, Nagoya University, Nagoya 464-8603, Japan

Received 18 March 2004; received in revised form 4 June 2004
Available online 30 July 2004

Abstract

Wave transmission characteristics in elastic media that have periodic microstructure over a finite spatial length are examined theoretically as well as numerically. Two classes of such media are demonstrated, namely, one-dimensional multilayered media with finite-length periodicity and two-dimensional composite media with square arrays of aligned fibers within a finite length. From these one-dimensional and two-dimensional analyses, the influence of the finite-length periodicity on the wave transmission characteristics is discussed. In these media, there are frequency bands (stop bands) where the energy transmission coefficient appears to vanish or takes very low values, while in pass bands it oscillates with the frequency due to the finite-length periodicity. It is theoretically demonstrated in the one-dimensional case of multilayers how the frequency intervals of the oscillation in the transmission spectrum depend on the repeating number of the periodic cells as well as other acoustic and geometrical parameters. The results of the two-dimensional fiber arrays, which are obtained numerically by solving the equations of the SH wave multiple scattering, are shown to fit well in the one-dimensional framework of multilayered structures up to a certain frequency encompassing the first stop band. This similarity between two classes of problems is demonstrated by appropriately identifying the one-dimensional reduced transfer matrix for a single cell that is representative of the periodic fiber array.

Keywords: Elastic wave; Periodic structure; Band gap; Energy transmission; Layered media; Transfer matrix; Fiber-reinforced composite; Multiple scattering

* Corresponding author. Present address: Department of Energy Conversion Science, Graduate School of Energy Science, Kyoto University, Yoshida-Honmachi, Sakyo-ku, Kyoto 606-8501, Japan. Tel.: +81 75 753 5897; fax: +81 75 753 5640.
E-mail address: biwa@energy.kyoto-u.ac.jp (S. Biwa).

0020-7683/$ - see front matter
doi:10.1016/j.ijsolstr.2004.06.017

1. Introduction

Wave propagation in periodic media such as multilayered structures has long been the subject of extensive research in various branches of optics, acoustics and elastodynamics, as documented by Brillouin (1953), Ewing et al. (1957) and Brekhovskikh (1960). Also, the elastic wave propagation in composite media with two- and three-dimensional periodic phase arrangements have been studied by many researchers, Nelson and Navi (1975), Kinra and Ker (1983), Kushwaha et al. (1993, 1994), Naciri et al. (1994), Suzuki and Yu (1998), Cai and Williams (1999), Henderson et al. (2001), to name but a few. In ideal situations where the microstructural periodicity extends over the whole space, one can resort to the so-called Bloch theorem and the analysis is reduced to the problem for a single unit cell. When the periodicity is of an incomplete nature, for example when the periodic arrangement is confined within a finite spatial domain, the analysis becomes cumbersome and remains as an intriguing topic of investigation.

Recently, Biwa et al. (2004) formulated a numerical scheme for multiple scattering of shear (SH) waves in unidirectional fiber composites based on the eigenfunction expansion and a collocation technique. Their procedure is capable of treating the multiple scattering by a number of fibers arranged either regularly or randomly. With this procedure, these authors examined the transmission spectra for the square as well as hexagonal fiber arrangements, and demonstrated that so-called stop bands were formed when the wave number satisfied a certain condition. Furthermore, the energy transmission coefficient in pass bands was found to oscillate with the frequency, with increasing amplitude and decreasing interval when approaching the edge of a stop band. This oscillatory behavior was considered to be due to the finite length of the region in which the fibers were arranged, but no decisive conclusions were drawn in that paper.

Understanding of such oscillatory nature in transmission spectra through finitely periodic media is important when analyzing their acoustic properties, since the repeatable number of periodic cells is inevitably finite in most situations. Such issues are attracting increasing attention regarding the application of so-called photonic crystals (Bendickson et al., 1996; Sakoda, 1997; Jeong et al., 2002), and their acoustic analogue of phononic band-gap structures (Page et al., 2001; Platts et al., 2002; Yang et al., 2002).

The present paper aims to explore the oscillatory response of the SH wave transmission in elastic media with microstructural periodicity of finite length from theoretical as well as numerical points of view. For this purpose, two classes of such media are considered, namely, one-dimensional layered media with finite-length periodicity and two-dimensional composites with square arrays of aligned fibers within a finite length. The former example, analyzed by the one-dimensional transfer matrix approach, offers a basic insight into the phenomenon at hand on a sound theoretical foundation. The latter example partly corresponds to the computational results in the previous paper (Biwa et al., 2004) but is reproduced here with finer frequency resolution in order to demonstrate the oscillation characteristics more clearly.

From these one-dimensional and two-dimensional analyses, the effect of the finite periodicity on the wave transmission characteristics is discussed. In particular, it is theoretically demonstrated in the one-dimensional case how the frequency intervals of the oscillation depend on the repeating number of the periodic cells as well as other acoustic and geometrical parameters. The features in the two-dimensional examples are examined based on the one-dimensional theoretical framework, by appropriately identifying the one-dimensional transfer matrix for a single cell that represents the periodic fiber array.

2. Wave transmission in multilayered structures of finite length

2.1. One-dimensional transfer matrix formulation

In this section, the wave propagation in multilayered structures is considered based on the one-dimensional transfer matrix formulation (Thomson, 1950; Haskell, 1953). The following derivation is similar to

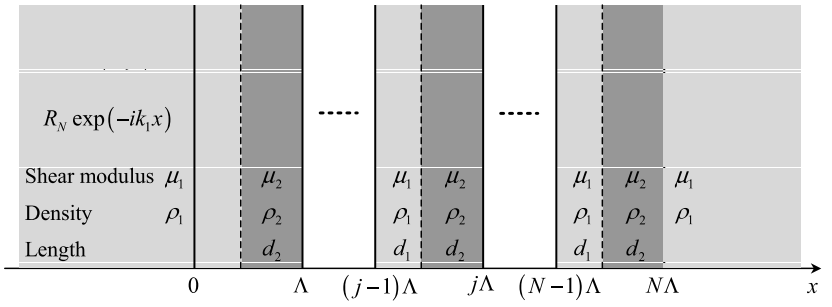

Fig. 1. One-dimensional periodic multilayered structure of finite length.

the work by Bendickson et al. (1996) that rests on a slightly different formulation. As shown in Fig. 1, the medium to be considered consists of an infinite elastic matrix (density ρ_1, shear modulus μ_1) with N embedded layers of dissimilar elastic solid (density ρ_2, shear modulus μ_2), which are of width d_2 and located with the equal spacing d_1 For the present formulation, it is convenient to regard this structure as the N-times repetition of a unit cell consisting of a matrix layer (referred to with the subscript 1) of length d_1 and a reinforcing layer (subscript 2) of length d_2 which is referred to as the N-cell layered structure. It is characterized by the periodic microstructure with period $\Lambda = d_1 + d_2$ and the total length $N\Lambda$ that is embedded in the infinite matrix.

The present analysis considers the elastic wave propagation in the x-direction taken normal to the layers with the out-of-plane polarization (SH wave). Then the governing equation for the one-dimensional displacement field $u(x)$ in the time-harmonic case with the angular frequency ω reduces to

$$\frac{\mathrm{d}^2 u}{\mathrm{d}x^2} + k_\alpha^2 u = 0 \tag{1}$$

for each layer, where

$$k_\alpha = \omega/c_\alpha, \quad c_\alpha = \sqrt{\mu_\alpha/\rho_\alpha} \tag{2}$$

are the wave number and the shear wave speed in each phase ($\alpha = 1, 2$). For convenience, the acoustic impedances are introduced as

$$W_\alpha = \rho_\alpha c_\alpha, \quad \alpha = 1, 2. \tag{3}$$

The continuity of the displacement as well as the shear traction at the boundaries between neighboring phases leads to the following matrix relation for the displacements and the shear stresses at the location $x = j\Lambda$ and $x = (j-1)\Lambda$, where $j = 1, 2, \ldots, N$:

$$\begin{Bmatrix} u(j\Lambda) \\ \tau(j\Lambda) \end{Bmatrix} = \mathbf{M} \begin{Bmatrix} u((j-1)\Lambda) \\ \tau((j-1)\Lambda) \end{Bmatrix}, \tag{4}$$

where $\mathbf{M}$ is the transfer matrix for a single cell and explicitly given by

$$\mathbf{M} \equiv \begin{bmatrix} M_{11} & M_{12} \\ M_{21} & M_{22} \end{bmatrix} = \begin{bmatrix} \cos\gamma_1 \cos\gamma_2 - (W_1/W_2)\sin\gamma_1 \sin\gamma_2 & (\sin\gamma_1 \cos\gamma_2/W_1 + \cos\gamma_1 \sin\gamma_2/W_2)/\omega \\ -\omega(W_1 \sin\gamma_1 \cos\gamma_2 + W_2 \cos\gamma_1 \sin\gamma_2) & \cos\gamma_1 \cos\gamma_2 - (W_2/W_1)\sin\gamma_1 \sin\gamma_2 \end{bmatrix}, \tag{5}$$

and the normalized wave numbers are defined as

$$\gamma_1 = k_1 d_1 = \omega d_1/c_1, \quad \gamma_2 = k_2 d_2 = \omega d_2/c_2. \tag{6}$$

It is noted that the origin $x=0$ has been taken as shown in Fig. 1, at the left boundary of the leftmost cell. A simple algebraic manipulation on the components of $\mathbf{M}$ in Eq. (5) shows

$$\det \mathbf{M} = M_{11}M_{22} - M_{12}M_{21} = 1. \tag{7}$$

2.2. Bloch phase for the infinite-cell layered structure

When the cells are infinitely repeated to cover the whole space ($N\to\infty$), the Bloch theorem states that the variables at adjacent cells are related as

$$\begin{Bmatrix} u(j\Lambda) \\ \tau(j\Lambda) \end{Bmatrix} = \mathrm{e}^{\mathrm{i}K\Lambda} \begin{Bmatrix} u((j-1)\Lambda) \\ \tau((j-1)\Lambda) \end{Bmatrix}, \tag{8}$$

where K is the Bloch wave number and $\beta = K\Lambda$ is referred to as the Bloch phase. Eqs. (4) and (8) constitute an eigenvalue problem for $\mathbf{M}$, where $\exp(\mathrm{i}K\Lambda)$ is identified as an eigenvalue of $\mathbf{M}$. With Eq. (7), it implies

$$(\mathrm{e}^{\mathrm{i}K\Lambda})^2 - (M_{11}+M_{22})\mathrm{e}^{\mathrm{i}K\Lambda} + 1 = 0, \tag{9}$$

which leads to

$$\cos(K\Lambda) = \frac{1}{2}(M_{11}+M_{22}) = \cos\gamma_1\cos\gamma_2 - \frac{W_1^2+W_2^2}{2W_1W_2}\sin\gamma_1\sin\gamma_2. \tag{10}$$

Namely, the Bloch phase $\beta = K\Lambda$ of the infinite-cell layered structure is related to the angular frequency ω and the parameters of the single cell, W_1, W_2, d_1/c_1 and d_2/c_2.

2.3. Transfer matrix for the N-cell layered structure

From the Cayley–Hamilton theorem applied to $\mathbf{M}$ and Eq. (9), it is seen that $\mathbf{M}$ satisfies the following matrix equation:

$$\mathbf{M}^2 - 2\cos\beta\mathbf{M} + \mathbf{I} = 0, \tag{11}$$

where $\mathbf{I}$ denotes the identity matrix. Furthermore, it can be shown from mathematical induction arguments (cf. Bendickson et al., 1996) that $\mathbf{M}^N$ is expressed by

$$\mathbf{M}^N = \frac{\sin N\beta}{\sin\beta}\mathbf{M} - \frac{\sin((N-1)\beta)}{\sin\beta}\mathbf{I}. \tag{12}$$

It is clear that $\mathbf{M}^N$ gives the transfer matrix for the N-cell layered structure, i.e.,

$$\begin{Bmatrix} u(N\Lambda) \\ \tau(N\Lambda) \end{Bmatrix} = \mathbf{M}\begin{Bmatrix} u((N-1)\Lambda) \\ \tau((N-1)\Lambda) \end{Bmatrix} = \cdots = \mathbf{M}^N \begin{Bmatrix} u(0) \\ \tau(0) \end{Bmatrix}. \tag{13}$$

From Eq. (12), the components of $\mathbf{M}^N$ are explicitly given as

$$\mathbf{M}^N \equiv \begin{bmatrix} M_{N11} & M_{N12} \\ M_{N21} & M_{N22} \end{bmatrix} = \frac{1}{\sin\beta}\begin{bmatrix} M_{11}\sin N\beta - \sin(N-1)\beta & M_{12}\sin N\beta \\ M_{21}\sin N\beta & M_{22}\sin N\beta - \sin(N-1)\beta \end{bmatrix}. \tag{14}$$

When the harmonic wave is incident on the N-cell layered structure in the positive x-direction (Fig. 1), the displacements outside the N cells are written as

$$u(x) = \exp(\mathrm{i}k_1x) + R_N\exp(-\mathrm{i}k_1x), \quad x\leqslant 0, \tag{15a}$$

$$u(x) = T_N \exp(\mathrm{i}k_1 x), \quad x \geqslant N\Lambda, \tag{15b}$$

and the corresponding shear stresses as $\tau(x) = \mu_1 \mathrm{d}u/\mathrm{d}x$, where R_N and T_N are the amplitude reflection and transmission coefficients for the N-cell layered structure. Substitution of these expressions into Eq. (13) gives T_N as

$$T_N = \frac{2\exp(-\mathrm{i}k_1 N\Lambda)}{M_{N11} + M_{N22} - \mathrm{i}(\omega W_1 M_{N12} - M_{N21}/(\omega W_1))}. \tag{16}$$

The energy transmission coefficient of the N-cell layered structure is simply calculated as

$$T_N^{\mathrm{e}} = T_N T_N^*, \tag{17}$$

where the asterisk $*$ denotes the complex conjugate.

When the absolute value of the rightmost-hand side of Eq. (10) does not exceed unity, the Bloch phase β is real. On the other hand, when it exceeds unity, β becomes complex and is written as

$$\beta = m\pi + \mathrm{i}\tilde{\beta} \quad (m = 1, 2, \ldots). \tag{18}$$

In this case, Eq. (12) can be rewritten as

$$\mathbf{M}^N = \frac{\cos mN\pi \sinh N\tilde{\beta}}{\cos m\pi \sinh \tilde{\beta}}\mathbf{M} - \frac{\cos(m(N-1)\pi)\sinh((N-1)\tilde{\beta})}{\cos m\pi \sinh \tilde{\beta}}\mathbf{I} \tag{19}$$

and T_N is still given by Eq. (16).

2.4. Energy transmission coefficient

From the above result, the energy transmission coefficient T_N^{e} of the N-cell layered structure is governed by the number of cells N, the impedance mismatch W_2/W_1, the ratio of the non-dimensional wave numbers (the ratio of the times of flight) in the two phases $\gamma_2/\gamma_1 = k_2 d_2/(k_1 d_1) = (d_2/c_2)/(d_1/c_1)$ as well as the normalized frequency ω/ω_0, where

$$\omega_0 = \frac{\pi}{(d_1/c_1 + d_2/c_2)} \tag{20}$$

corresponds to the angular frequency at which the reflected waves from neighboring cells interfere constructively. It is noted that when $(d_2/c_2)/(d_1/c_1) = 1$, the periodic structure meets the so-called quarter-wave stack condition (Bendickson et al., 1996).

In order to demonstrate the influence of the three parameters listed above, the case with $N = 10$, $W_2/W_1 = 1.5$ and $(d_2/c_2)/(d_1/c_1) = 1$ is taken as a reference, and the frequency dependence of the energy transmission coefficient of the N-cell layered structure is computed by varying one parameter while keeping the other two unchanged. Figs. 2–4 show the computed results for the influences of the cell number N (Fig. 2), the impedance mismatch W_2/W_1 (Fig. 3), and the time-of-flight ratio $(d_2/c_2)/(d_1/c_1)$ (Fig. 4).

In Fig. 2, three curves with $N = 5$, 10 and 20 exhibit a stop band at $\omega/\omega_0 = 1$. It is seen that the transmission coefficient is very low for $N = 5$ and nominally vanishes for $N = 10$ and 20 in this stop band. Furthermore, the edge of the stop band is sharper for larger N. Outside of the stop band (in pass bands), the three curves oscillate against the frequency, with increasing amplitude as the frequency approaches $\omega/\omega_0 = 1$. It is also seen that the frequency interval of the oscillation is smaller when the cell number N is larger. In Fig. 3, three results with $W_2/W_1 = 1.25$, 1.5 and 2 are shown, where the band gap opens wider and the oscillation amplitude is greater when the impedance mismatch is greater. Finally, Fig. 4 shows four curves with $(d_2/c_2)/(d_1/c_1) = 1$, 1.1, 1.5 and 2 in a wider frequency range up to $\omega/\omega_0 = 3.5$. It is seen that the occurrence of stop bands depends remarkably on $(d_2/c_2)/(d_1/c_1)$. Namely, although the energy transmission

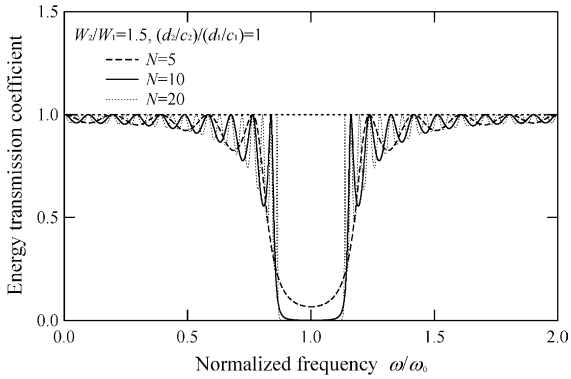

Fig. 2. Energy transmission spectra of the one-dimensional multilayer for different cell numbers.

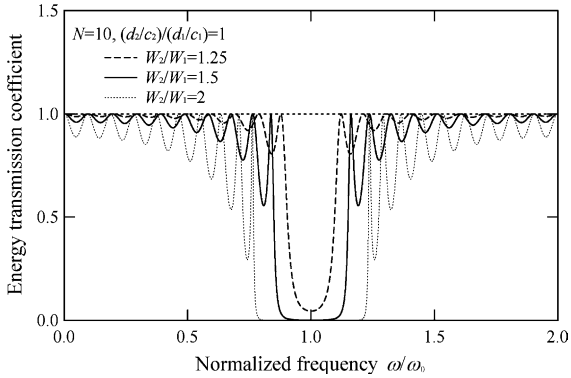

Fig. 3. Energy transmission spectra of the one-dimensional multilayer for different impedance ratios.

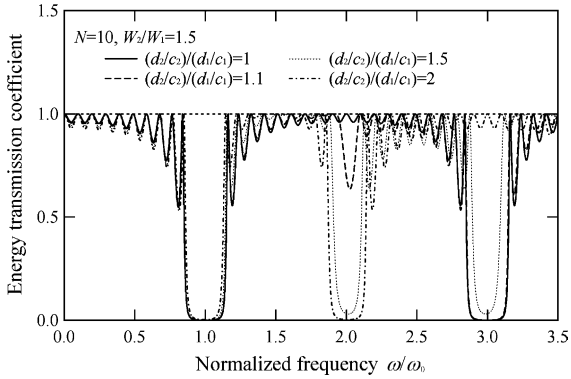

Fig. 4. Energy transmission spectra of the one-dimensional multilayer for different time-of-flight ratios.

coefficients for $(d_2/c_2)/(d_1/c_1) = 1.1$ and 1.5 exhibit stop bands at the frequencies $\omega/\omega_0 = 1$, 2 and 3, the result with $(d_2/c_2)/(d_1/c_1) = 1$ lacks a band gap at $\omega/\omega_0 = 2$, and that with $(d_2/c_2)/(d_1/c_1) = 2$ lacks one at $\omega/\omega_0 = 3$, due to the negative interference of the reflected waves from the interface within each cell.

3. Wave transmission through periodic fiber arrangements of finite length

3.1. Fundamental equations of SH wave multiple scattering

In this section, the time-harmonic SH wave propagation in a two-dimensional composite with periodic fiber arrangements of a finite spatial length is considered. The matrix (shear modulus μ_1 and density ρ_1) and the fibers (μ_2, ρ_2 and radius a) are assumed homogeneous and isotropic, and the wave numbers as well as the velocities in both phases are given by Eq. (2) with the subscripts 1 and 2 now being interpreted to represent the matrix and the fiber, respectively. The time-harmonic wave field $u(x_1, x_2)$ in this composite obeys the two-dimensional scalar Helmholtz equation:

$$\left(\frac{\partial^2}{\partial x_1^2}+\frac{\partial^2}{\partial x_2^2}\right)u + k_\alpha^2 u = 0, \quad \alpha = 1, 2. \tag{21}$$

It is assumed that the fiber-reinforced region consists of the repetition of fundamental blocks with length L and height H as shown in Fig. 5. In the fundamental block, total of N_f fibers are arranged to form a square lattice, containing N vertical columns of fibers. For example, in the particular arrangement shown in Fig. 5, $N=26$ and $N_f=6N=156$. The blocks with the same fiber arrangement are repeated infinitely in the x_2-direction to build up the whole fiber arrangement. Such arrangements are analogous to the N-cell layered structure considered in Section 2, and referred to as the N-cell fiber arrangement.

In the multiple scattering theory (Waterman and Truell, 1961), the wave field that impinges on a generic fiber is called the exciting field to that fiber, and given by the sum of the incident wave $u^{\text{inc}}(\boldsymbol{r}) = \exp(\mathrm{i}k_1 x_1)$ and the scattered waves from all the other fibers. The exciting field $u_i^{\text{exc}}(\mathbf{r})$ for the fiber with its center located at $\mathbf{r}_i$ can be expanded using eigenfunctions of the Helmholtz equation with respect to the origin at $\mathbf{r}_i$, i.e.,

$$u_i^{\text{exc}}(\mathbf{r}) = u^{\text{inc}}(\mathbf{r}) + \sum_{\substack{j \\ j\neq i}} u_j^{\text{sca}}(\mathbf{r}) = \sum_{n=-\infty}^{\infty} a_n^i J_n(k_1|\mathbf{r}-\mathbf{r}_i|)\exp(\mathrm{i}n\theta_i), \tag{22}$$

where $J_n(\cdot)$ is the nth order Bessel function of the first kind, θ_i is the angle from $\mathbf{r}_i$ to $\mathbf{r}$, and the summation for the integer j is taken for all fibers but the one at $\mathbf{r}_i$.

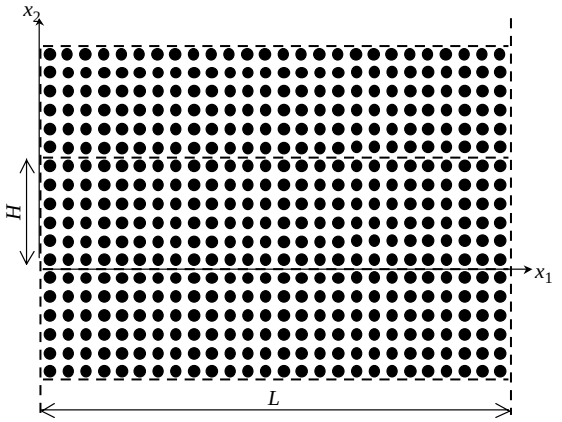

Fig. 5. Two-dimensional composite with square fiber arrangement of finite length.

The scattered wave from the fiber at $\mathbf{r}_i$ can be expanded as

$$u_i^{\mathrm{sca}}(\mathbf{r}) = \sum_{n=-\infty}^{\infty} b_n^i H_n(k_1|\mathbf{r}-\mathbf{r}_i|)\exp(\mathrm{i}n\theta_i), \tag{23}$$

where $H_n(\cdot)$ is the nth order Hankel function of the first kind. Based on the notion of transfer matrix related to the scattering by a single fiber (Waterman, 1969), the expansion coefficients of the scattered wave b_n^i can be related to those of the exciting field a_n^i as

$$b_n^i = T_n^{\mathrm{sca}} a_n^i, \quad T_n^{\mathrm{sca}} = \frac{\mu_1 k_1 J_n'(k_1 a) J_n(k_2 a) - \mu_2 k_2 J_n(k_1 a) J_n'(k_2 a)}{\mu_2 k_2 H_n(k_1 a) J_n'(k_2 a) - \mu_1 k_1 H_n'(k_1 a) J_n(k_2 a)} \tag{24}$$

for a circular fiber, where the prime denotes the derivative with respect to the argument.

3.2. Computational procedure

Owing to the perfect periodicity in the x_2-direction, the wave field in the medium due to the plane wave incidence in the x_1-direction becomes periodic in the x_2-direction, and the fibers aligned in the same vertical column suffer the same exciting field. Therefore, the governing equations for the multiple scattering problem can be formulated in terms of the N_f fibers in one fundamental block. In this situation, substitution of Eqs. (23) and (24) into Eq. (22) gives

$$\begin{aligned}\sum_{n=-\infty}^{\infty} a_n^i J_n(k_1|\mathbf{r}-\mathbf{r}_i|)\exp(\mathrm{i}n\theta_i) = \exp(\mathrm{i}k_1\mathbf{r}) &+ \sum_{p=-\infty}^{\infty}\sum_{\substack{j=1\\ j\neq i}}^{N_f}\sum_{m=-\infty}^{\infty} T_m^{\mathrm{sca}} a_m^j H_m(k_1|\mathbf{r}-(\mathbf{r}_j+pH\mathbf{i}_2)|)\exp(\mathrm{i}m\theta_{jp}) \\ &+ \sum_{\substack{p=-\infty\\ p\neq 0}}^{\infty}\sum_{m=-\infty}^{\infty} T_m^{\mathrm{sca}} a_m^i H_m(k_1|\mathbf{r}-(\mathbf{r}_i+pH\mathbf{i}_2)|)\exp(\mathrm{i}m\theta_{ip}),\end{aligned} \tag{25}$$

Eq. (25) holds at arbitrary points in the matrix, and consists of the infinite sums over the parameters n (m) and p. If the wavelength is sufficiently large compared to the radius and spacing of the fibers, the analysis requires only a few leading terms of the eigenfunction expansions in Eqs. (22) and (23). When these expansions are truncated at a finite level, i.e. up to $n=\pm n_{\max}$ and likewise for m, Eq. (25) contains $N_f\times(2n_{\max}+1)$ unknown coefficients a_n^i. To determine these unknown variables, Eq. (25) is evaluated at $(2n_{\max}+1)$ collocation points for each of N_f fibers, and the resulting system of linear equations is solved numerically. Furthermore, the infinite sums with respect to the parameter p are also truncated at a finite but sufficiently large value in the numerical procedure, since the terms with large $|p|$ corresponds to the effect of remote fibers whose influence may be negligible as $|p|\to\infty$. The truncation levels for p are chosen large enough not to influence the numerical results at reasonable computational costs, depending on the frequency involved in each problem. For more details, readers are referred to the previous paper (Biwa et al., 2004).

It is noted in passing that in principle the analysis of the square arrays at hand only needs a fundamental block containing one fiber in the x_2-direction, owing to the periodicity in this direction. Such a small fundamental block saves the computational cost significantly as the number of unknown variables becomes much smaller. Otherwise the choice of the fiber number in x_2-direction is not essential, as the numerical parameter p in Eq. (25) has to be chosen accordingly so as to simulate the infinitely repeated nature. In our present study, the 6×10 and 6×26 arrays have been chosen as they also serve as a reference to which the influence of the perturbed fiber arrangement on the wave transmission behavior is studied numerically, as will be reported elsewhere.

3.3. Energy transmission coefficient

The energy transmission coefficients through the fiber-reinforced region have been computed for different incident frequencies, assuming the acoustic properties relevant to the Ti-alloy matrix ($\mu_1 = 45$ GPa, $\rho_1 = 5400$ kg/m^3) and the SiC fibers ($\mu_2 = 177$ GPa, $\rho_2 = 3200$ kg/m^3) (cf. Rokhlin et al., 1995; Biwa and Shibata, 2000). The fibers are arranged as a square lattice in the fundamental block with the ratio of center-to-center fiber spacing d to the fiber radius a as $d/a = 3.545$ resulting in the fiber volume fraction in the block to be $\phi = \pi a^2/d^2 = 0.25$.

Fig. 6(a) and (b) show the results for the model consisting of 10 fiber columns (10-cell fiber arrangement) and that with 26 columns as shown in Fig. 5 (26-cell fiber arrangement), respectively, where the angular frequency is normalized as $(d/c_1)\omega$. In this figure, the energy transmission coefficient has been calculated as the ratio $\langle e\rangle(x_1)/\langle e\rangle_0$, where $\langle e\rangle(x_1)$ is the time-averaged energy flow in the x_1-direction in the reinforced medium averaged also in the x_2-direction, and $\langle e\rangle_0$ is the corresponding quantity in the absence of the fibers, namely the energy flux density of the incident wave (Biwa et al., 2004).

$$T_N^{\mathrm{e}} \equiv \frac{\langle e\rangle(x_1)}{\langle e\rangle_0} = -\frac{1}{H}\frac{\mathrm{i}\omega}{4}\int_{-H/2}^{H/2}\left\{\mu\frac{\partial u}{\partial x_1}u^* - \left(\mu\frac{\partial u}{\partial x_1}\right)^* u\right\}\mathrm{d}x_2 \Big/ \left(\frac{1}{2}\omega k_1\mu_1\right), \tag{26}$$

where $\mu = \mu_1$ or μ_2 depending on the position on the integration path. Being defined this way, T_N^{e} should be independent of the coordinate x_1 which serves as a check for the numerical accuracy, although it has been evaluated at $x_1 = 1.1\ L$ in accordance with the previous study (Biwa et al., 2004).

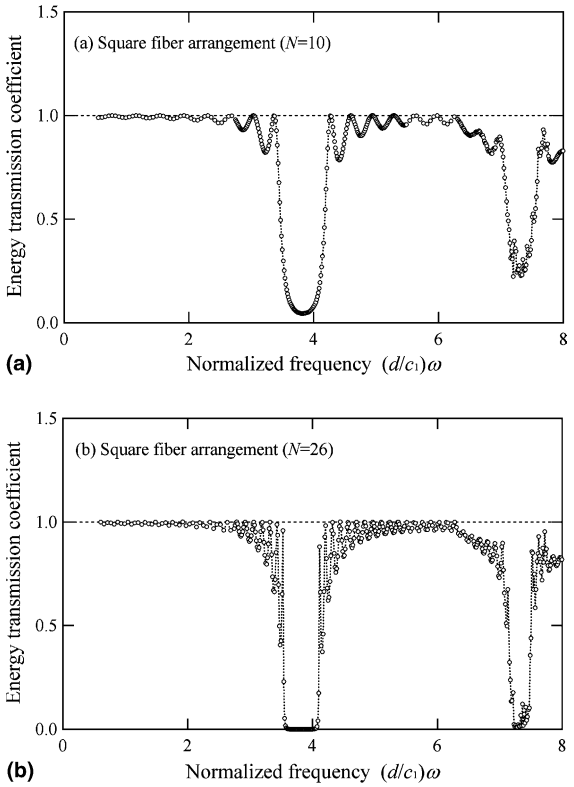

Fig. 6. Energy transmission spectra for (a) the 10-cell fiber arrangement and (b) the 26-cell fiber arrangement.

For these fiber arrays, the first stop band appears when the wave number k that arises in the reinforced region meets the condition $kd=\pi$, and so does the second stop band when $kd=2\pi$ (Biwa et al., 2004). In the case of 10-cell fiber arrangement, the energy transmission coefficient falls to low levels in the first and second stop bands. In the 26-cell fiber arrangement, the energy transmission appears to vanish completely in the first stop band, though the second stop band is not as complete as the first one. Furthermore, significant oscillation of the energy transmission coefficient with the frequency is appreciable in both cases. The frequency intervals of the oscillation are much smaller in the 26-cell arrangement than in the 10-cell arrangement.

4. Discussion

4.1. One-dimensional multilayered structures

In the foregoing sections, it has been demonstrated that the energy transmission coefficient of the finitely periodic structures exhibit oscillatory behavior against the frequency in both one-dimensional and two-dimensional cases. Moreover, the oscillation has been observed to be quite remarkable near the edge of a stop band.

From Eqs. (14) and (16), the energy transmission coefficient in the one-dimensional problem discussed in Section 2 is shown to take the value of unity, namely, the full transmission occurs, when

$$\beta=\cos^{-1}\left(\cos\gamma_1\cos\gamma_2-\frac{W_1^2+W_2^2}{2W_1W_2}\sin\gamma_1\sin\gamma_2\right)=\frac{n\pi}{N},\quad n=1,2,\ldots,N-1, \tag{27}$$

for the first pass band, since at these points Eqs. (12) and (16) reduce to

$$\mathbf{M}^N=-\frac{\sin(N-1)\beta}{\sin\beta}\mathbf{I} \tag{28}$$

and

$$T^N=\pm\exp(-\mathrm{i}k_1N\Lambda). \tag{29}$$

Clearly, these points are equally spaced in $\beta\in(0,\pi)$. Bendickson et al. (1996) have also pointed out this constant-interval nature of full-transmission points in the β space in the context of one-dimensional photonic crystals assuming a quarter-wave stack. The numerical examples shown in Section 2 all conform to this observation. Namely, in Fig. 2, the 5-cell, 10-cell, and 20-cell layered structures have 4, 9, and 19 full-transmission points, respectively, in the first pass band.

The above feature is now examined in more details for the one-dimensional case that permits a rigorous analysis. Eq. (10) defines the relation between the Bloch phase β and the angular frequency of the incident wave ω. This relation is shown in Fig. 7 for different values of W_2/W_1 using representative parameter of $(d_2/c_2)/(d_1/c_1)=1$. It should be noted that this relation does not depend on the cell number N. From (10), $\mathrm{d}\beta/\mathrm{d}\omega$ in the low-frequency limit is given by

$$\lim_{\omega\to0}\frac{\mathrm{d}\beta}{\mathrm{d}\omega}=\left(\frac{d_1^2}{c_1^2}+\frac{d_2^2}{c_2^2}+\frac{W_1^2+W_2^2}{W_1W_2}\frac{d_1d_2}{c_1c_2}\right)\frac{\omega}{\beta}. \tag{30}$$

The above expression implies that in the β–ω plane, the curve defined by Eq. (10) approaches the straight line of the slope C, defined by

$$C\equiv\lim_{\omega\to0}\frac{\mathrm{d}\beta}{\mathrm{d}\omega}=\sqrt{\frac{d_1^2}{c_1^2}+\frac{d_2^2}{c_2^2}+\frac{W_1^2+W_2^2}{W_1W_2}\frac{d_1d_2}{c_1c_2}}. \tag{31}$$

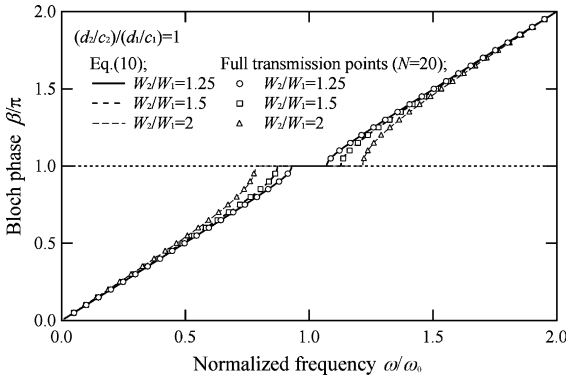

Fig. 7. Variation of the Bloch phase with the normalized frequency for the one-dimensional multilayer.

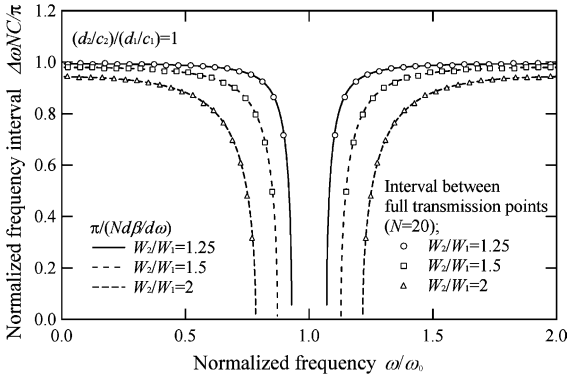

Fig. 8. Variation of the interval between full-transmission points with the normalized frequency for the one-dimensional multilayer.

On the other hand, as β approaches π from downwards, one observes $\mathrm{d}\beta/\mathrm{d}\omega \to \infty$.

In the β space, the $(N-1)$ full-transmission points with $T_N^{\mathrm{e}} = 1$ are located with the same interval π/N from Eq. (27). In Fig. 7, such points in the case of $N=20$ are illustrated as symbols together with the theoretical curves of Eq. (10). When the frequency is sufficiently low (when β is sufficiently small), the corresponding interval in the ω space is evaluated as $\pi/(NC)$ using the slope C introduced above. As $\beta \to \pi$, however, the frequency interval becomes smaller. Fig. 8 shows the plot of the frequency interval of neighboring full-transmission points $\Delta\omega$ (normalized by the low-frequency limit $\pi/(NC)$) as a function of the center frequency of each interval. The plots appear to fall on a continuous curve given by $g(\omega) \equiv \pi/(N\mathrm{d}\beta/\mathrm{d}\omega)$, which is governed by the parameters of the single cell, W_1, W_2, d_1/c_1 and d_2/c_2. Therefore, the frequency interval of the oscillation becomes narrower as the edge of the stop band is approached. Moreover, this effect is more appreciable when the cell number N is larger.

4.2. Two-dimensional fiber arrangements

Turning our attention to the two-dimensional fiber-reinforced media, the results shown in Section 3 reveal some features much similar to those clarified above for the one-dimensional multilayers. Namely, the full-transmission points in Fig. 6 appear to divide the frequency range from 0 to the edge of the first stop band into 10 and 26 intervals for the 10-cell and 26-cell fiber arrangements, respectively, although

the numerical nature of the plots makes the precise identification of full-transmission points somewhat ambiguous.

In order to highlight the similarity as well as the difference between the one-dimensional multilayers and the two-dimensional fiber arrays, the latter problem is now reduced to the one-dimensional problem in the following way, in order to see which features in the two-dimensional results fit in the one-dimensional theory and which do not. To this purpose, the wave field for a single vertical column of the fibers, that is, the 1-cell fiber arrangement of the length $\Lambda = d$ as shown in Fig. 9(a), is analyzed by the computational procedure outlined in Section 3. Then, the obtained wave field $u(x_1, x_2)$ in this two-dimensional problem is averaged for the x_2-direction to obtain the reduced one-dimensional wave field,

$$\bar{u}(x_1) \equiv \frac{1}{H}\int_0^H u(x_1, x_2)\,\mathrm{d}x_2. \tag{32}$$

The complex amplitude transmission and reflection coefficients T_1 and R_1 of the 1-cell fiber arrangement are then identified from the above reduced wave field using the following relations:

$$T_1 = \frac{\bar{u}(\Lambda)}{\exp(\mathrm{i}k_1\Lambda)}, \quad R_1 = \bar{u}(0) - 1. \tag{33}$$

With the stress–displacement relation in the matrix $\bar{\tau}(x_1) = \pm\mathrm{i}\mu_1 k_1 \bar{u}(x_1)$ for the forward (+) and backward (−) propagation, the one-dimensional transfer matrix expression similar to Eq. (4) is given by

$$\begin{Bmatrix} T_1\exp(\mathrm{i}k_1\Lambda) \\ \mathrm{i}\mu_1 k_1 T_1 \exp(\mathrm{i}k_1\Lambda) \end{Bmatrix} = \begin{bmatrix} M_{11} & M_{12} \\ M_{21} & M_{22} \end{bmatrix} \begin{Bmatrix} 1 + R_1 \\ \mathrm{i}\mu_1 k_1 (1 - R_1) \end{Bmatrix} \tag{34}$$

for the variables at $x_1 = 0$ and $x_1 = \Lambda$. Likewise, if the time-reversal process of the above problem as shown in Fig. 9(b) is considered (Bendickson et al., 1996), one obtains the following relation:

$$\begin{Bmatrix} T_1^*\exp(-\mathrm{i}k_1\Lambda) \\ -\mathrm{i}\mu_1 k_1 T_1^* \exp(-\mathrm{i}k_1\Lambda) \end{Bmatrix} = \begin{bmatrix} M_{11} & M_{12} \\ M_{21} & M_{22} \end{bmatrix} \begin{Bmatrix} 1 + R_1^* \\ -\mathrm{i}\mu_1 k_1 (1 - R_1^*) \end{Bmatrix}, \tag{35}$$

where T_1^* and R_1^* are the complex conjugates of T_1 and R_1 respectively.

From Eqs. (34) and (35), it is possible to determine the four components of the transfer matrix **M** in terms of T_1 and R_1. If the components of **M** are identified for different frequencies in this manner, Eq. (10) in the one-dimensional theory gives the relation between the Bloch phase and the incident angular frequency for the square fiber array at hand. This is demonstrated in Fig. 10, which shows a behavior similar to Fig. 7 in the one-dimensional multilayers, exhibiting jumps of the frequency at $\beta = \pi$ and $\beta = 2\pi$.

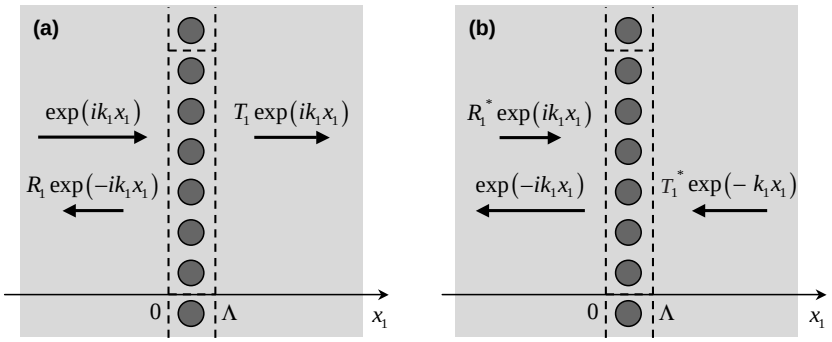

Fig. 9. Wave propagation in the 1-cell fiber arrangement: (a) the forward problem and (b) its time-reversal problem.

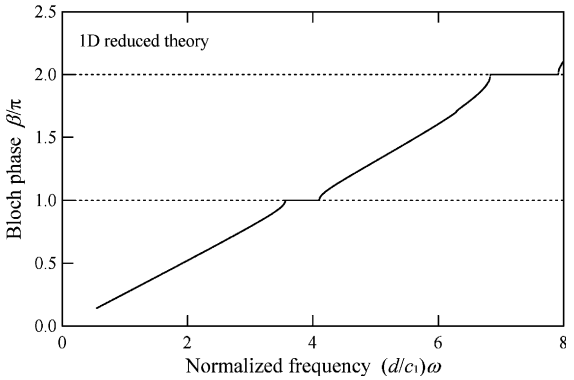

Fig. 10. Variation of the Bloch phase with the normalized frequency for the fiber array obtained by the reduced one-dimensional theory.

It is now possible to obtain the transfer matrix for N cells from Eq. (12). Then, the wave transmission spectrum of the two-dimensional N-cell fiber arrangement can be calculated by Eqs. (16) and (17) from the above transfer matrix of the 1-cell fiber arrangement, if the one-dimensional theory is applicable. Fig. 11(a)

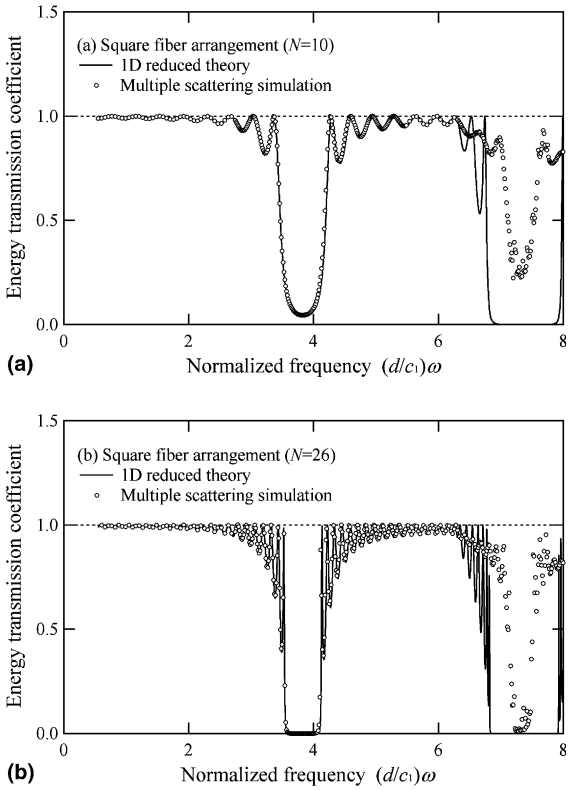

Fig. 11. Energy transmission spectra for (a) the 10-cell fiber arrangement and (b) the 26-cell fiber arrangement, predicted by the reduced one-dimensional theory.

and (b) show the so-constructed transmission spectra for the 10-cell and 26-cell fiber arrangements, respectively, as solid lines. For comparison, the results from the direct multiple scattering simulation shown in Fig. 6 are also plotted as symbols. It is quite remarkable that both results agree extremely well in the low-frequency range up to about $(d/c_1)\omega = 6$, which encompasses the first stop band. Especially, the oscillation patterns of the transmission coefficients as well as the first stop-band profiles are very accurately reproduced by the reduced one-dimensional theory.

From Fig. 11, it is also clear that the transmission spectra of the reduced theory start to differ significantly from those based on the direct multiple scattering simulation when the frequency exceeds the level of about $(d/c_1)\omega = 6$. In particular, the reduced theory predicts the opening of very wide band gaps at $kd = 2\pi$ (second stop band) for both $N = 10$ and $N = 26$, while the direct simulation gives narrower (26-cell fiber arrangement) or shallower (10-cell fiber arrangement) band gaps. This discrepancy indicates the failure of the one-dimensional reduced theory at such high frequencies. The energy transmission through the fiber arrays predicted by the direct multiple scattering simulation in this frequency range is likely due to the fiber-to-fiber interactions in oblique directions, which cannot be resolved within the framework of the one-dimensional theory. Further analysis seems to be needed in order to fully understand the success/failure of the one-dimensional theory depending on the frequency range.

5. Conclusion

Wave transmission characteristics in periodic media of finite length have been examined from theoretical as well as numerical points of view. Two examples of such media have been considered, namely, one-dimensional multilayered media with finite-length periodicity and two-dimensional square arrays of aligned fibers within a finite length. From these one-dimensional and two-dimensional analyses, the influence of the finite length of the periodic microstructure on the wave transmission characteristics has been discussed.

References

Bendickson, J.M., Dowling, J.P., Scalora, M., 1996. Analytic expressions for the electromagnetic mode density in finite, one-dimensional, photonic band-gap structures. Physical Review E 53, 4107–4121.

Biwa, S., Shibata, T., 2000. Elastic and ultrasonic properties of a unidirectional composite with partially debonded fibres: numerical analysis for longitudinal shear modes. Composites Science and Technology 60, 83–93.

Biwa, S., Yamamoto, S., Kobayashi, F., Ohno, N., 2004. Computational multiple scattering analysis for shear wave propagation in unidirectional composites. International Journal of Solids and Structures 41, 435–457.

Brekhovskikh, L.M., 1960. Waves in Layered Media. Academic Press, New York.

Brillouin, L., 1953. Wave Propagation in Periodic Structures. Dover, New York.

Cai, L.-W., Williams Jr., J.H., 1999. Full-scale simulations of elastic wave scattering in fiber-reinforced composites. Ultrasonics 37, 463–482.

Ewing, W.M., Jardetzky, W.S., Press, F., 1957. Elastic Waves in Layered Media. McGraw-Hill, New York.

Haskell, N.A., 1953. The dispersion of surface waves on multilayered media. Bulletin of the Seismological Society of America 43, 17–34.

Henderson, B.K., Maslov, K.I., Kinra, V.K., 2001. Experimental investigation of acoustic band structures in tetragonal periodic particulate composite structures. Journal of the Mechanics and Physics of Solids 49, 2369–2383.

Jeong, D.-Y., Ye, Y.H., Zhang, Q.M., 2002. Effective optical properties associated with wave propagation in photonic crystals of finite length along the propagation direction. Journal of Applied Physics 92, 4194–4200.

Kinra, V.K., Ker, E.L., 1983. An experimental investigation of pass bands and stop bands in two periodic particulate composites. International Journal of Solids and Structures 19, 393–410.

Kushwaha, M.S., Halevi, P., Dobrzynski, L., Djafari-Rouhani, B., 1993. Acoustic band structure of periodic elastic composites. Physical Review Letters 71, 2022–2025.

Kushwaha, M.S., Halevi, P., Martínez, G., Dobrzynski, L., Djafari-Rouhani, B., 1994. Theory of acoustic band structure of periodic elastic composites. Physical Review B 49, 2313–2322.

Naciri, T., Navi, P., Ehrlacher, A., 1994. Harmonic wave propagation in viscoelastic heterogeneous materials: Part I. Dispersion and damping relations. Mechanics of Materials 18, 313–333.

Nelson, R.B., Navi, P., 1975. Harmonic wave propagation in composite materials. Journal of the Acoustical Society of America 57, 773–781.

Page, J.H., Goertzen, A.L., Yang, S., Liu, Z., Chan, C.T., Sheng, P., 2001. Acoustic band gap materials. In: Soukoulis, C.M. (Ed.), Photonic Crystals and Light Localization in the 21st Century. Kluwer Academic Publishers, Amsterdam, pp. 59–68.

Platts, S.B., Movchan, N.V., McPhedran, R.C., Movchan, A.B., 2002. Two-dimensional phononic crystals and scattering of elastic waves by an array of voids. Proceedings of the Royal Society of London A 458, 2327–2347.

Rokhlin, S.I., Huang, W., Chu, Y.C., 1995. Ultrasonic scattering and velocity methods for characterization of fibre–matrix interphases. Ultrasonics 33, 351–364.

Sakoda, K., 1997. Numerical analysis of the interference patterns in the optical transmission spectra of a square photonic lattice. Journal of the Optical Society of America B 14, 1961–1966.

Suzuki, T., Yu, P.K.L., 1998. Complex elastic wave band structures in three-dimensional periodic elastic media. Journal of the Mechanics and Physics of Solids 46, 115–138.

Thomson, W.T., 1950. Transmission of elastic waves through a stratified solid medium. Journal of Applied Physics 21, 89–93.

Waterman, P.C., 1969. New formulation of acoustic scattering. Journal of the Acoustical Society of America 45, 1417–1429.

Waterman, P.C., Truell, R., 1961. Multiple scattering of waves. Journal of Mathematical Physics 2, 512–536.

Yang, S., Page, J.H., Liu, Z., Cowan, M.L., Chan, C.T., Sheng, P., 2002. Ultrasound tunneling through 3D phononic crystals. Physical Review Letters 88, 104301-1-4.